

# Prediction of Thermoacoustic Instabilities: Numerical Study of Mach number Effects.

K. Wieczorek\*

*CERFACS, 31057 Toulouse, France*

F. Nicoud†

*Université Montpellier II - I3M CNRS UMR 5149, 34095 Montpellier , France*

This paper presents a method for the prediction of combustion instability in gas turbine combustion chambers. The framework of this study are the Linearized Euler Equations formulated in the frequency domain as an eigenvalue problem. Flame-acoustic interaction is considered using an  $n - \tau$ -model. Making no assumptions about the mean flow field and the shape of the eigenmodes, the approach is applicable to complex geometries. The appearance and convection of entropy waves and as well as their interaction with the acoustic field in regions of non-uniform mean flow are taken into account.

Based on prior work, the concept is applied to 1D and 2D academic test configurations. The impact of a non zero Mach number mean flow on the frequency of oscillation and growth rate of resonant modes is analysed. Results obtained with the Linearized Euler Equations solver are compared to and validated by results of a semi-analytical method, as well as by computations carried out with a time domain flow solver for the compressible Euler equations.

## I. Introduction

In the calculation of thermoacoustic instabilities, an assumption that is commonly made is that of the mean flow velocity being small enough to be considered zero. This allows to considerably simplify the Linearized Euler Equations (LEE), which are used to describe the phenomenon of acoustic propagation, and to derive one single wave equation. However, this zero Mach number assumption may lead to significant changes in the evaluation of the thermo-acoustic modes present in the combustion chamber. This is especially the case when the mean flow is not isentropic, which is always given in combustion applications. In such configurations, entropy waves (hot spots) are generated in the flame region and convected downstream. In regions of accelerated mean flow they may interact with the acoustic field and be partly converted into acoustic waves, which may then propagate upstream<sup>1</sup>.

The numerical prediction of thermoacoustic instabilities is subject of extensive research, which has lead to the development of a number of different approaches. The methods differ in the degree of simplification and modeling applied to the conservation equations, which is reflected in their computational cost. A direct solution of the complete Navier-Stokes equations, including chemical reactions in the combustion zone, allows to capture all relevant driving and damping mechanisms<sup>2</sup>. However, the demand in computation time and memory of LES computations is often too high to be a viable option for industrial configurations. A somewhat opposite approach is represented by network models. They are based on a simplified description of the configuration in terms of acoustic elements with piecewise uniform meanflow, where the coupling of flame and acoustic field is described by a model<sup>3,4</sup>. These methods allow to characterize complex systems by only a small number of parameters and are therefore particularly suitable for extensive preliminary studies or as "demonstration devices" for modelling approaches. Yet, their lack in geometrical precision prevents their application to more complex configurations. An intermediate approach both in terms of modelling and computational cost consists in solving a set of linearized equations using finite volume or finite element

---

\*Ph.D. Student, CERFACS, 42, Av. G. Coriolis, Toulouse

†Professor, Math Department, Place Eugène Bataillon, Montpellier

methods<sup>5-8</sup>. This allows to represent arbitrary geometries and mean flow conditions, but still requires an appropriate description of the flame's interaction with the acoustic field.

The present study is based on this latter approach, solving the Linearized Euler Equation in the frequency domain. In difference to time domain simulations, where the unsteady field is dominated by the most amplified (or least damped) mode, calculations in the frequency domain allow to capture and analyze the first modes of a configuration independently of their growth rate. The interaction of flame and acoustic field is described using an  $n - \tau$ -model, which allows to express the unsteady heat release of the flame in terms of the acoustic variables. The system of equations can then be written as an eigenvalue problem, which is solved using the Arnoldi algorithm.

In the present paper, this approach is applied to 1D and 2D academic test configurations, extending prior work on 1D and quasi-1D configurations.<sup>9,10</sup>

## II. Model

The equations used to describe the acoustic field are derived from the conservation laws of mass, momentum and energy:

$$\frac{D\rho}{Dt} = -\rho\nabla \cdot \mathbf{u} \quad (1)$$

$$\rho \frac{D\mathbf{u}}{Dt} = -\nabla p \quad (2)$$

$$\frac{Ds}{Dt} = \frac{rq}{p} \quad (3)$$

where  $\rho$ ,  $p$ ,  $T$ ,  $\mathbf{u}$  and  $s$  denote density, static pressure, static temperature, velocity vector and entropy respectively. The quantity  $r = C_p - C_v$  is the specific gas constant of the fluid and  $q$  the heat release per unit volume.

The acoustic equations can then be derived by decomposing the instantaneous values of density, velocity vector, pressure and entropy into a steady mean flow (index 0) and fluctuations of small amplitude (index 1), in the form  $\phi(\mathbf{x}, t) = \phi_0(\mathbf{x}) + \phi_1(\mathbf{x}, t)$ . Introducing this decomposition into Eqs. (1)- (3) and keeping only terms of first order leads to the Linearized Euler Equations. Assuming the fluctuating quantities to be harmonic in time, they can be expressed as  $\phi_1(\mathbf{x}, t) = \Re(\hat{\phi}(\mathbf{x})e^{-i\omega t})$ , with the complex frequency  $\omega = \omega_r + i\omega_i$  describing frequency and growth rate of the perturbations. The Linearized Euler Equations can then be noted in a frequency domain formulation:

$$(\nabla \cdot \mathbf{u}_0 + \mathbf{u}_0 \cdot \nabla)\hat{\rho} + (\nabla\rho_0 + \rho_0\nabla) \cdot \hat{\mathbf{u}} = i\omega\hat{\rho} \quad (4)$$

$$\left(\frac{\nabla c_0^2}{\rho_0} + \frac{\mathbf{u}_0 \cdot \nabla \mathbf{u}_0}{\rho_0} + \frac{c_0^2}{\rho_0}\nabla\right)\hat{\rho} + (\nabla\mathbf{u}_0 \cdot + \mathbf{u}_0 \cdot \nabla)\hat{\mathbf{u}} + (\gamma - 1)T_0\left(\frac{\nabla p_0}{p_0} + \nabla\right)\hat{s} = i\omega\hat{\mathbf{u}} \quad (5)$$

$$\frac{\gamma r q_0}{\rho_0 p_0}\hat{\rho} + \nabla s_0 \cdot \hat{\mathbf{u}} + \left(\mathbf{u}_0 \cdot \nabla + (\gamma - 1)\frac{q_0}{p_0}\right)\hat{s} - \frac{r}{p_0}\hat{q} = i\omega\hat{s} \quad (6)$$

In the above equations,  $c_0$  denotes the mean speed of sound and  $\gamma = C_p/C_v$  the heat capacity ratio. The linearized state equation and entropy expression read:

$$\frac{\hat{p}}{p_0} - \frac{\hat{\rho}}{\rho_0} - \frac{\hat{T}}{T_0} = 0 \quad (7)$$

$$\frac{\hat{s}}{C_v} = \frac{\hat{p}}{p_0} - \gamma \frac{\hat{\rho}}{\rho_0} \quad (8)$$

The interaction between the flame and the acoustic field is described using a  $n - \tau$ -model<sup>5,11,12</sup>. This model relates the local unsteady heat release  $\hat{q}(\mathbf{x})$  to an interaction index  $n_u(\mathbf{x})$ , a time lag  $\tau$  and a reference acoustic velocity immediately upstream of the flame  $\hat{\mathbf{u}}_{\mathbf{x}_{\text{ref}}}$ :

$$\hat{q}(\mathbf{x}) = \frac{q_{\text{total}}}{U_{\text{bulk}}} n_u(\mathbf{x}) e^{i\omega\tau} \hat{\mathbf{u}}_{\mathbf{x}_{\text{ref}}} \cdot \mathbf{n}_{\text{ref}} \quad (9)$$

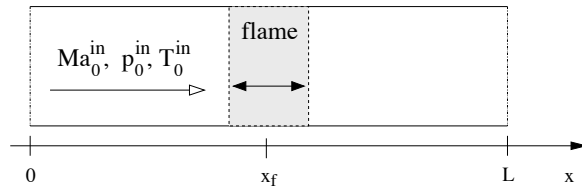


Figure 1: 1D test case configuration

with  $\mathbf{n}_{\text{ref}}$  a unitary vector defining the direction of the reference velocity. In this expression, the quantities  $U_{\text{bulk}}$  and  $q_{\text{total}}$  are the bulk velocity and total heat release, respectively. The local interaction index is further defined as

$$n_u(x) = \frac{n}{\delta_f} \frac{U_{\text{bulk}}}{q_{\text{total}}} \frac{\gamma}{\gamma-1} p_0 \quad \text{for } x_f - \frac{\delta}{2} < x < x_f + \frac{\delta}{2}; \quad (10)$$

$$n_u(x) = 0 \quad \text{otherwise}$$

with  $\delta_f$  being the flame thickness.

Expressing the unsteady heat release in terms of the acoustic variables allows to write the system of equations (4) - (6) as an eigenvalue problem of the form

$$\mathcal{A}\mathcal{V} = i\omega\mathcal{V} \quad (11)$$

where the matrix  $\mathcal{A}$  is a linear operator applied to the eigenvector  $\mathcal{V} = (\hat{\rho}, \hat{\mathbf{u}}, \hat{s})^T$ , and  $\omega = \omega_r + i\omega_i$  the complex eigenvalue.

In discrete form, the problem of Eq. (11) becomes

$$[A][V] = i\omega[V] \quad (12)$$

where the discrete eigenvector  $[V]$  contains the unknown values of  $(\hat{\rho}, \hat{\mathbf{u}}, \hat{s})^T$  for each grid point.

The numerical solution of the eigenvalue problem is obtained using the Arnoldi method. In order to improve the convergence towards the eigenvalues of physical interest (i.e. those close to zero), the Arnoldi method is applied to the shifted and inverted problem.

Note that in cases with unsteady heat release, the operator matrix  $[A]$  depends on  $\omega$  via Eq. (9). The discretised eigenvalue problem has then to be solved iteratively. Starting from the value for  $\omega$  obtained for  $\hat{q} = 0$ , convergence is usually obtained after 3 to 4 computations.

### III. 1D Study

In the 1D-equivalent of Eqs. (4)-(9), the velocity vector  $\mathbf{u}(\mathbf{x})$  is reduced to its component in  $x$ -direction, which will be noted  $u(x)$  in the following. The number of unknowns in the eigenvector reduces to three per grid point, i.e.  $[V]$  contains now  $(\hat{\rho}, \hat{u}, \hat{s})$ .

In order to generate the operator matrix  $[A]$ , the domain is discretized by a grid of about 1000-2000 equidistant points. Gradients of  $\hat{\rho}$  and  $\hat{u}$  are then approximated using a central finite difference scheme, while gradients of  $\hat{s}$  are expressed using an upwind difference scheme. In order to avoid numerical instability, a staggered grid formulation is used, with values of  $\hat{u}$  being stored at the nodes, while  $\hat{\rho}$  and  $\hat{s}$  are stored at the cell centers.

The configuration to be considered consists in a tube of length  $L$  with constant cross section, which contains a 1D-flame of thickness  $\delta_f$  at position  $x_f$  (see Fig. 1). The mean flow field is imposed via an analytical distribution of static temperature of the form

$$T_0(x) = \frac{T_0^{\text{out}} + T_0^{\text{in}}}{2} + \frac{T_0^{\text{out}} - T_0^{\text{in}}}{2} \tanh\left(3 \frac{x - x_f}{\frac{1}{2}\delta_f}\right) \quad (13)$$

$p_0^{in}$ (Pa)	$T_0^{in}$ (K)	$T_0^{out}$ (K)	$\gamma$	$r$ (J/kgK)	$L$ (m)	$x_f/L$
101325	300	1200	1.4	287	1.0	0.5

Table 1: Physical parameters used for the calculations concerning the configuration of Fig. 1.

	$\delta_f \rightarrow 0$	$\delta_f/L = 0.05$	$\delta_f/L = 0.10$
1	$92.6 - 7.4i$	$91.3 - 7.8i$	$93.7 - 7.5i$
2	$347.2 - 0.1i$	$360.8 + 6.7i$	$372.3 + 14.0i$
3	$582.4 + 53.2i$	$582.0 + 55.1i$	$580.9 + 50.9i$

Table 2: First three eigen frequencies of the configuration of Fig. 1 at  $M_0^{in} = 0.001$ .

where  $x_f$  and  $\delta_f$  denote the position and thickness of the flame respectively. The conservation laws for mass flux, momentum and total temperature provide the conditions  $\rho_0 u_0 = \text{const.}$ ,  $p_0 + \rho_0 u_0^2 = \text{const.}$  and  $q_0 = \rho_0 u_0 C_p dT_{t0}/dx$ , where  $T_{t0}$  is the total temperature of the mean flow. The flow field is then entirely defined by the choice of inlet pressure  $p_0^{in}$ , temperature  $T_0^{in}$ , Mach number  $M_0^{in}$  and a temperature step  $T_0^{out} - T_0^{in}$ . The mean flow parameters used for this test case are gathered in Table 1.

The unsteady heat release of the flame is modeled using the  $n - \tau$ - model of Eqs. (9) and (10) with the parameters  $n = 3$  and  $\tau = 0.5\text{ms}$ . The boundary conditions are set to  $\hat{s} = 0$  and  $\hat{u} + u_0/(\rho_0 c_0^2)\hat{p} = 0$  at the inlet  $x = 0$  and to  $\hat{p} + \rho_0 u_0 \hat{u} = 0$  at the outlet  $x = L$ . The conditions for the acoustic waves are thus set in a way that the acoustic energy flux across the domain boundaries  $F = (\hat{u} + u_0/(\rho_0 c_0^2)\hat{p})(\hat{p} + \rho_0 u_0 \hat{u})$  is zero at both inlet and outlet<sup>13</sup>. As for the entropy wave, the boundary condition implies that any entropy fluctuations present in the domain are created in the flame and then convected downstream.

Computations with the LEE solver have been carried out for two values of flame thickness,  $\delta_f/L = 0.05$  and  $\delta_f/L = 0.10$ . The results of these calculations are validated using a semi-analytical model presented by Dowling<sup>14</sup>, which solves the problem for the limit case  $\delta_f \rightarrow 0$ .

The eigenfrequencies of the first three modes as calculated by the semi-analytical method and by the LEE solver are gathered in Table 2 for a mean flow being virtually at rest. The LEE computations predict results that show overall good agreement with the semi-analytical model, the results for the shorter flame being closer to those obtained using the infinitely thin flame assumption. The impact of the flame thickness on the eigenfrequency is not equally strong for the three modes. The second mode is especially sensitive to changes in flame thickness, which is due to the fact that this mode presents a velocity node near the flame zone. As this is also the position where the reference velocity for the flame model is determined, small changes in the velocity field may have an important effect.

In the following, the third eigenmode is further analyzed, varying the mean flow Mach number at the domain inlet. Figure 2 shows the complex eigenfrequencies of the third mode of this configuration for Mach numbers increasing from  $M_0^{in} = 0.001$  to  $M_0^{in} = 0.15$  obtained from the LEE solver ( $\diamond$ -symbols for  $\delta_f/L = 0.05$ ,  $\triangle$ -symbols for  $\delta_f/L = 0.10$ ) and the semi-analytical model ( $\bullet$ -symbols).

For the mean flow being at rest, the two methods predict virtually the same result, irrespective of the thickness of the flame zone. When the mean flow is taken into account, the LEE results differ clearly from those of the semi-analytical model, even though they converge towards those latter when the flame thickness is reduced from  $\delta_f/L = 0.10$  ( $\triangle$ -symbols) to  $\delta_f/L = 0.05$  ( $\diamond$ -symbols).

Both methods predict a general trend towards lower real frequencies and more stability when the mean flow velocity is increased. However, the LEE calculations, that resolve the flame, predict a transition from an unstable mode ( $\omega_i > 0$ ) to a stable mode ( $\omega_i < 0$ ) for high mean flow velocities, which is not the case for the calculations based on the semi-analytical model. For this configuration, the transition from the initially (i.e. at  $M_0^{in} = 0.001$ ) unstable third mode to a stable mode occurs at lower mean flow velocities when the flame thickness is increased.

The structure of the third eigenmode obtained from the LEE calculations for a flame thickness of  $\delta_f/L =$

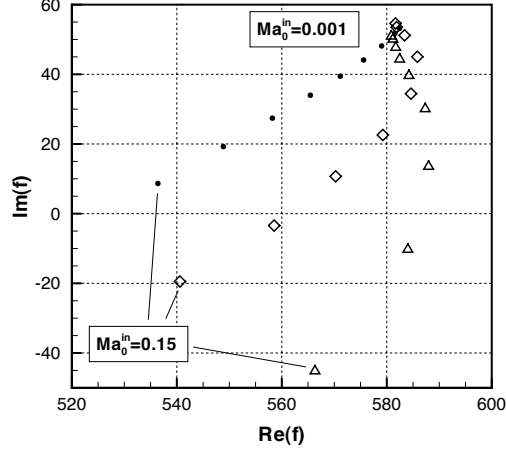


Figure 2: Evolution of the complex frequency of the 3rd mode with increasing mean flow Mach number and flame thickness. Parameters of flame-acoustic interaction model:  $n = 3$ ,  $\tau = 0.5\text{ms}$ .

•: semi-analytical method ( $\delta_f \rightarrow 0$ ),  $\diamond$ : LEE ( $\delta_f/L = 0.05$ ),  $\triangle$ : LEE ( $\delta_f/L = 0.10$ )  
for  $M_0^{\text{in}} = 0.001$  and  $M_0^{\text{in}} = 0.01$  to  $0.15$  in steps of  $\Delta M_0^{\text{in}} = 0.02$ .  $\text{Im}(f) > 0$ : unstable,  $\text{Im}(f) < 0$ : stable.

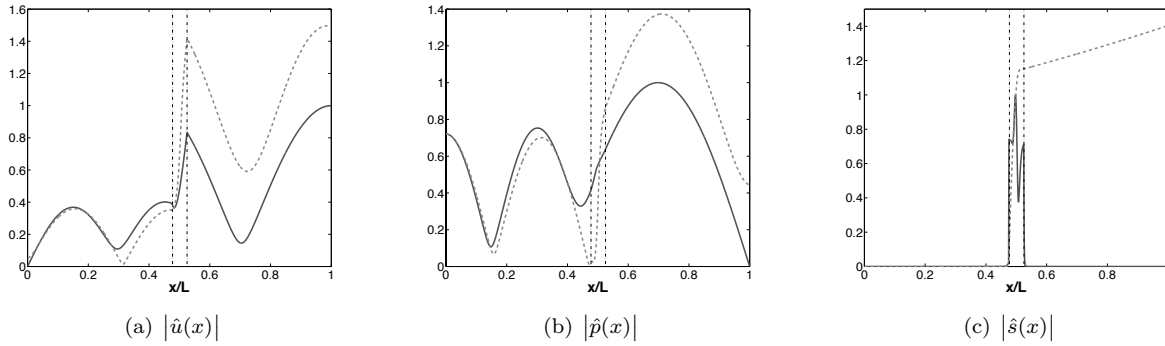


Figure 3: Form of the third eigenmode for  $M_0^{\text{in}} = 0.001$  (solid line;  $f_{0.001} = 581.7 + 54.6i$  Hz) and  $M_0^{\text{in}} = 0.15$  (dashed line;  $f_{0.15} = 540.6 - 19.5i$  Hz) for  $\delta_f/L = 0.05$ . The dash-dot lines mark the position of the flame.

0.05 and for inlet mean flow velocities of  $M_0^{\text{in}} = 0.001$  and  $M_0^{\text{in}} = 0.15$  is shown in Fig. 3. While the inlet Mach number has almost no effect upstream on the flame, the mode shape changes clearly in the flame region and downstream of the flame. The most noticeable change can be observed for the distribution of fluctuating entropy (see Fig. 3(c)): When the mean flow is assumed to be at rest, these fluctuations are not only confined to the flame zone, but the amount of fluctuating entropy created in the flame zone is underpredicted.

## IV. 2D Study

The 1D study shows that the effect of the mean flow on the resonant frequencies and the form of the modes is not always negligible. However, a 1D solver is restricted to rather simple configurations. In order to be applicable to more complex geometries, the approach is implemented in a 2D solver.

The numerical tool designed for the 2D analysis solves the system of equations (4)-(6) using a second order finite volume scheme. The appearance of point-to-point instabilities which is inherent to this method is avoided by the addition of an artificial viscosity term. This term is based on the formulation used in the LES solver AVBP.<sup>15</sup> As this latter, the presented 2D solver uses a cell-vertex discretization for unstructured grids. In difference to the second order discretization used for the system of equations (4)-(6), the artificial viscosity term is of fourth order in space. This is achieved by a computation of gradients in several steps,



Figure 4: Mesh used for the 2D computation of the 1D-flame configuration. Marker: reference point for  $n - \tau$ -model at  $x = 0.47\text{m}$ .

which allows to build a centered five point stencil. The resulting term has then the form of a fourth order derivative, and is noted  $d\Phi^{AV}$  when applied to a given quantity  $\Phi$ :

$$d\Phi^{AV} = \eta \frac{\partial^4 \Phi}{\partial \mathbf{x}^4}$$

The complete expression of this term, noted here in 1D for the sake of simplicity, reads

$$d\Phi^{AV} = \eta \frac{\partial^4 \Phi}{\partial x^4} = \eta \frac{(\Phi_{n-2} - 4\Phi_{n-1} + 6\Phi_n - 4\Phi_{n+1} + \Phi_{n+2})}{(\Delta x)^4} \quad \text{with} \quad \eta = \epsilon_4 \frac{|u + c|}{16} (\Delta x)^3$$

where  $\Phi_n$ ,  $\Phi_{n-1}$ , etc. denote the values of the quantity  $\Phi$  at points  $n$ ,  $n - 1$ , etc.;  $\Delta x$  a characteristic length scale describing the cell size of the grid and  $u$  and  $c$  the mean flow speed and speed of sound respectively. Finally,  $\epsilon_4$  is a user-defined value that allows to adjust the amplitude of the artificial viscosity term, which must of course be small compared to the other terms of the system.

The artificial viscosity operator is then applied to each of the components of the discrete eigenvector  $[V] = (\hat{\rho}, \hat{\mathbf{u}}, \hat{s})^T$ . The resulting term is introduced into the system of equations (4) - (6), transforming Eq. (12) into

$$[A][V] + \eta \frac{\partial^4 [V]}{\partial \mathbf{x}^4} = i\omega[V] \quad (14)$$

Eq. (14) shows that the description of the system in the form of an eigenvalue problem is maintained, the problem reading now:

$$[A + \eta \frac{\partial^4}{\partial \mathbf{x}^4}][V] = i\omega[V] \quad (15)$$

The introduction of an artificial viscosity term in an otherwise inviscid problem is certainly not without controversy. This method therefore has to be used with caution, in order not to modify the behaviour of the system. The approach is nonetheless justified, as the presented study is concerned with resonant modes rather than acoustic propagation. Unlike in the case of acoustic propagation problems, where waves may traverse distances much larger than their wavelength, the wavelengths of the resonant eigenmodes considered in this study are of the same order as the length of the combustion chamber. Errors due to the introduction of an artificial viscosity term are therefore small enough so as to not be prohibitive for the presented analysis.

## A. 1D Flame

As a first test case, the configuration presented in the 1D study is computed with the 2D solver. The mean flow field, flame model parameters and boundary conditions correspond to those of section III. The flame zone covers a length of  $\delta_f/L = 0.05$ . The domain is discretized using about 8700 triangular cells, the mesh being refined in the flame zone (see Fig. 4).

Computations have been carried out for inlet Mach numbers of  $M_0^{\text{in}} = 0.001$  and  $M_0^{\text{in}} = 0.15$ . The results are compared to those obtained with the 1D solver. The computations of the 1D solver are carried out on a grid of 1000 equidistant points, which corresponds to a uniform cell size of  $\Delta x = 0.001\text{m}$ . For the 2D mesh, a cell sizes of about  $\Delta x = 0.001\text{m}$  is only reached in the flame zone, whereas near the boundaries the mesh is coarser with a cell size of the order of  $\Delta x = 0.01\text{m}$ .

The eigenfrequencies obtained for the third mode are noted in Table 3. The results of the 1D and 2D solvers show good agreement, for the frequencies of oscillation as well as for the growth rates.

A comparison of the mode shapes obtained with the 1D and 2D solver is shown in Fig. 5. The spatial distribution for the modules of pressure, velocity and entropy fluctuations is shown for a mean flow with velocity close to zero. As entropy fluctuations are restricted to the flame zone when the mean flow is at

	f (Hz) 1D Solver	f (Hz) 2D Solver
$M = 0.001$	$582.0 + 55.1i$	$581.9 + 54.0i$
$M = 0.15$	$540.6 - 19.5i$	$539.2 - 20.7i$

Table 3: Comparison of 1D and 2D solver: Eigenfrequency of the third mode of the 1D-flame configuration at low and high Mach number for  $\delta_f/L = 0.05$ .

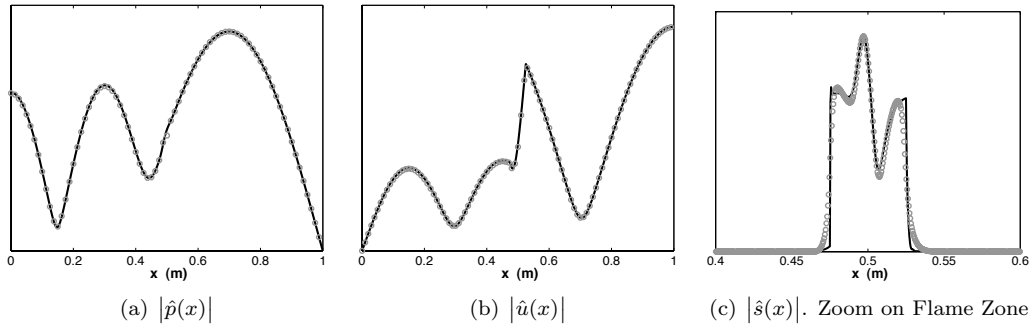


Figure 5: Comparison of mode shape at  $M_0^{\text{in}} = 0.001$  obtained by 1D and 2D solvers for the 1D-flame configuration. Solid Line: 1D solver. Circles: 2D solver.

rest, their spatial distribution involves steep gradients on both sides of the flame zone, that have to be captured appropriately. When convection is accounted for, the convected entropy waves are structures with a wavelength much shorter than the acoustic wavelength, by a factor that corresponds to the mean flow Mach number:  $\lambda_e/\lambda_{ac} = u/c = M$ . This emphasizes that especially at low Mach numbers, discretization is an important issue.

## B. Nozzle Flow

As a second test case for the 2D LEE solver, the flow through a tube connected to a choked isentropic nozzle is investigated. A flame and therefore entropy fluctuations are not considered here, which allows to discretize the domain with a coarser mesh. The domain has a total length of  $L = 2\text{m}$  and is discretized using about 2800 triangular cells, the mesh being refined around the nozzle throat that is located at  $x_{th} = 1.65\text{m}$  (see Fig. 6).

The mean flow field of this configuration is determined numerically. The mean flow Mach number at the domain inlet is of about  $M_0^{\text{in}} = 0.11$ . After an acceleration in the nozzle, the flow reaches  $M = 1$  at the nozzle throat and is supersonic across the complete outlet section. The distribution of mean Mach number, temperature and pressure are shown in Fig. 7.

The results obtained by the LEE solver are validated by time domain computations carried out with the flow solver AVBP<sup>15</sup>. This code provides the possibility to solve the compressible Euler equations on unstructured grids. The approach used for comparison of the results between the two codes is the following:

1. The mean flow field is determined using the time domain solver.
2. Based on the mean flow field determined by the time domain flow solver, the LEE solver computes resonant frequencies, growth rates and mode shapes of the first resonant modes.
3. At the same time, the frequencies of the resonant modes are determined using the time domain flow solver. To this end, the flow field has to be excited in a suitable way. One possibility is to launch the calculation imposing a perturbation on one single node in the region upstream of the nozzle throat, e.g. an increased value for mean pressure. Another option is to excite the field at its inlet boundary, adding a time-periodic signal of small amplitude to one of the inlet conditions. This time-periodic signal is composed of a sum of  $N$  sinusoids covering the frequency range to be investigated, i.e. a finite Fourier series with a sufficiently small fundamental frequency  $f_0$  and harmonics of equal amplitude  $\epsilon$

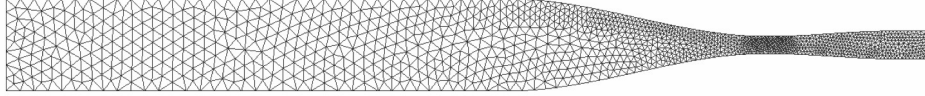


Figure 6: Mesh used for the computation of a choked nozzle flow.

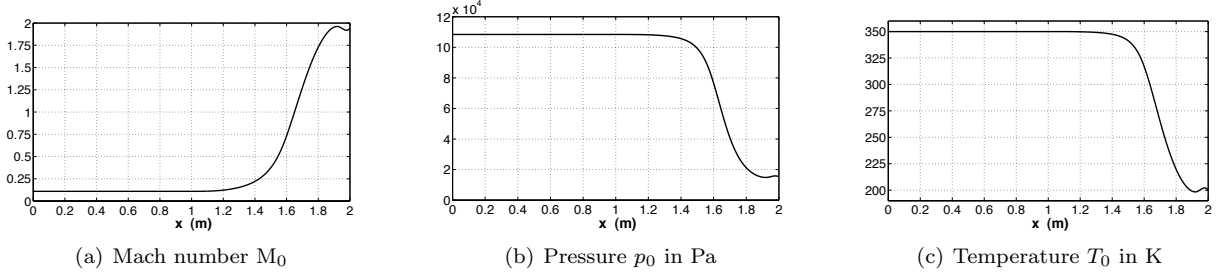


Figure 7: Mean flow field obtained for the choked nozzle configuration.

up to the maximum frequency of interest  $f_{max} = Nf_0$ , of the form

$$\phi(\mathbf{x}_{inlet}, t) = \phi_0(\mathbf{x}_{inlet}, t) \left( 1 + \epsilon \sum_{n=1}^N \sin(2\pi n f_0 t) \right) \quad (16)$$

The perturbation needs to be of small amplitude, so that the error due to disturbing the boundary condition can be considered negligible.

In order to determine the resonant frequencies of the domain, it is then sufficient to capture the temporal evolution of a flow variable, e.g. pressure or velocity, at a suitable location. Those are the areas where the fluctuations in the respective quantities are expected to be maximal. Adapted positions are indicated in the mode shapes determined by the LEE solver. The temporal evolution of these quantities contains information about the frequencies that respond to the excitation. These frequencies can then be determined by applying a Fourier transform to the respective result signal.

4. Finally, the time domain solver is used to verify the growth rate of one of the modes computed by the LEE solver. As the flow field of the time domain flow solver is dominated by the least damped mode, only the growth rate of this latter can be determined. To this end, the distribution of fluctuating quantities at an initial time  $t_0 = 0$  is reconstructed from the mode shape and resonant frequency determined by the LEE solver (step 2). As introduced in section II, the expression that links the frequency domain and the time domain fields reads  $\phi_1(\mathbf{x}, t) = \Re(\hat{\phi}(\mathbf{x})e^{-i\omega t})$ . The field  $\phi_1(\mathbf{x}, t_0)$  being determined this way, it is superimposed to the mean flow as initial perturbation of small amplitude  $\epsilon$ , such that  $\phi(\mathbf{x}, t_0) = \phi_0(\mathbf{x}, t_0) + \epsilon\phi_1(\mathbf{x}, t_0)$ . As the frequency domain LEE solver does not give any information about the amplitude of the perturbations, an arbitrary but small value for  $\epsilon$ , of the order of 1-5% of the mean flow values, is applied.

Starting the time domain computation with this initial field, the decay rate of the mode that is investigated can directly be determined by following the temporal evolution of the perturbation.

In order to realize this comparison and interaction of a time-domain flow solver and a frequency-domain code for acoustics, the boundary conditions used in the two codes have to be compatible.

At the outlet, the supersonic mean flow sets the boundary condition for both the time domain and frequency domain solvers. As no information can travel upstream in a supersonic flow, it is not meaningful to impose any boundary values at the outlet. This means also that for the acoustic solver, the domain is implicitly restricted to the part upstream of the nozzle throat. Even though the part of the domain downstream of the nozzle throat is included in the computation, it does not have an influence on the results for the resonant frequencies.

	f (Hz) (domain Fig. 6)	f (Hz) (extended domain)
1	$132.79 - 7.50i$	$132.74 - 7.42i$
2	$259.31 - 17.60i$	$259.32 - 17.53i$
3	$375.36 - 35.93i$	$375.38 - 35.85i$

Table 4: First eigenvalues of the choked nozzle configuration obtained by the 2D LEE solver.

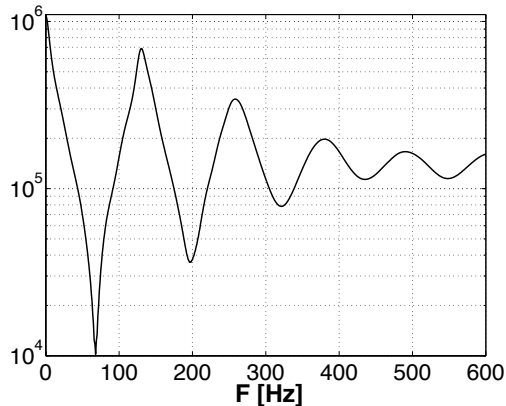


Figure 8: Discrete Fourier Transform of the pressure signal at the domain inlet. Maximum response is obtained at the frequencies  $f_1 = 131\text{Hz}$ ,  $f_2 = 259\text{Hz}$ ,  $f_3 = 379\text{Hz}$ .

At the inlet, the time domain solver requires information about the mass flow rate  $\dot{m}(t)$  that enters the domain. In terms of acoustic variables, fixing the mass flow rate means suppressing any fluctuations of that quantity, i.e.  $\dot{m}' = (\rho u)' = 0$ . For the acoustic solver, this corresponds to a boundary condition that sets the acoustic flux to zero, i.e.  $u_0 \hat{\rho} + \rho_0 \hat{u} = 0$ . As mentioned before, entropy fluctuations are not considered here, so as second inlet condition for the acoustic solver one finds  $\hat{s} = 0$ .

In order to capture the resonant frequencies of the domain and to verify the growth rate of a mode (steps 3 and 4), the boundary conditions of the time-domain flow solver have to be reflecting for acoustic waves. This issue is addressed in the solver AVBP by the use of characteristic boundary conditions (NSCBC<sup>16</sup>).

Based on the mean flow field described above, the results for the steps 2-4 are the following:

**STEP 2:** The values obtained by the 2D LEE solver for the complex eigenfrequencies of the first three modes are gathered in Table 4. As no source terms for acoustic energy are present in the domain, but acoustic energy is convected outside of the domain, all modes are damped.

These results have been checked by a second computation, for which the domain was extended by 0.5m beyond the initial outlet (see Table 4, right column). As this extension is situated beyond the sonic nozzle throat, it may not have an influence on the resonant frequencies of the domain. The results obtained for the extended domain being virtually the same as those of the initial computation, they confirm that the passage to supersonic flow is correctly captured by the solver.

**STEP 3:** The resonant frequencies of the domain are then computed by the time domain flow solver. The excitation of the flow field is achieved by adding a small amplitude signal as described above (cf. Eq. (16)) to the mass flow rate at the inlet. The response is captured by recording the pressure signal near the domain inlet, as all modes feature a pressure maximum at this position. After the mean pressure is subtracted from the signal, a discrete Fourier transform is carried out, yielding the result displayed in Fig. 8.

The resonant frequencies of the domain determined this way are of  $f_1 = 131\text{ Hz}$ ,  $f_2 = 259\text{ Hz}$  and  $f_3 = 379\text{ Hz}$ . These values correspond very well to those determined by the LEE solver. The high damping rates for the higher order modes are reflected in the Fourier transform plot in Fig. 8 by less pronounced peaks for the 2nd and 3rd mode.

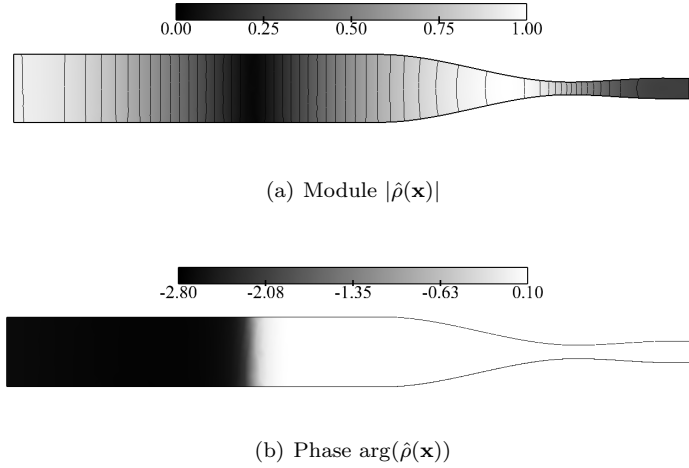


Figure 9: Spatial structure of the first eigenmode.

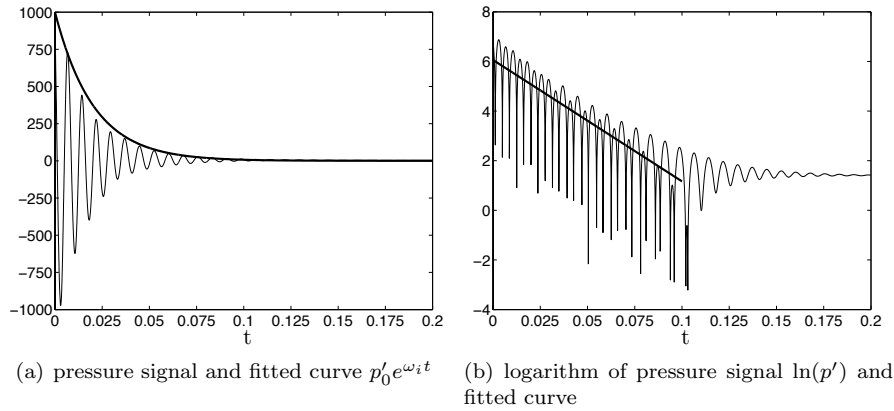


Figure 10: Temporal evolution of pressure signal at domain inlet for first eigenmode.

STEP 4: Finally, the damping rate of the least damped mode is verified by the time-domain flow solver. In this case, the mode to be analyzed is the first longitudinal mode of the configuration, whose shape is illustrated via phase and argument of the density fluctuations in Fig. 9. As entropy is not present in this case, the distribution of density and pressure are of the same form. The mode being superimposed to the mean flow field, the pressure signal is again recorded at the domain inlet, i.e. at a point of maximum pressure. The pressure signal obtained this way is plotted in Fig. 10(a).

The first mode has a cycle increment of  $\zeta = \exp\left(\frac{2\pi\omega_i}{\omega_r}\right) - 1 = -0.299$ , meaning that the amplitude of the perturbation decreases by about 30% per period. Thus, the signal is damped after very few oscillations, which limits the precision of the damping rate determined by fitting a curve directly to the signal. The pressure signal is therefore plotted on a logarithmic scale in Fig. 10(b), with a linear curve being deduced using a linear regression on the maximum values of  $|p'|$ , taking into account the time from  $t = 0$  to  $t = 0.1$ s. The value determined this way from the flow solver is of  $\omega_i \approx -7.8$  Hz, which is in good agreement with the result predicted by the LEE solver.

Besides, the fact that the pressure signal at the inlet follows very neatly a function of the form  $\cos(\omega_r t)e^{\omega_i t}$  indicates that the first mode that is introduced as initial condition oscillates without irregularities. This way, the transfer of the field of fluctuating quantities from the LEE solver to the time domain flow solver confirms the mode shape that has been determined.

The results found by the time domain solver show hence overall good agreement with those of the LEE solver, confirming that all relevant terms are correctly taken into account.

## V. Conclusion

This article presents a modal analysis of academic configurations, based on solving the Linearized Euler Equations in the frequency domain. Accounting for mean flow effects and flame acoustic coupling, the presented method aims at improving the prediction of combustion instability. In difference to other common techniques, no assumptions about the mean flow or the shape of the eigenmodes are made.

The approach is first applied to a 1D configuration, the set of linearized equations being solved using a finite difference technique. The results obtained by this finite difference solver show good agreement with a semi-analytical model. It is shown that a non zero mean flow velocity may considerably change the growth rate of a mode, among others by losses at the domain outlet due to convected entropy fluctuations.

In order to consider more complex geometries, a 2D code has been developed subsequently. The Linearized Euler Equations are discretized using a finite volume technique on unstructured grids. It is shown that the task of numerical instability may be handled using an artificial viscosity term.

For the 2D frequency domain solver, a validation methodology allowing its comparison to a time domain flow solver is presented. On the example of the flow through a choked nozzle it is shown that resonant frequencies and the growth rate of the least damped mode are predicted with acceptable accuracy. The presented approach allows to use directly the well defined acoustic boundary condition that is set by a sonic nozzle throat. In difference to zero Mach number approaches, preliminary computation of the nozzle behaviour is avoided.

## Acknowledgments

K.W. is grateful to the European Community for funding her PhD work under the project AETHER (Contract No. FP6 - MRTN-CT-2006-035713).

## References

- <sup>1</sup>F. E. Marble and S. Candel. Acoustic Disturbances from Gas Non-Uniformities Convected Through a Nozzle. *J. Sound Vib.* , 55:225–243, 1977.
- <sup>2</sup>C. Martin, L. Benoit, Y. Sommerer, F. Nicoud, and T. Poinsot. LES and Acoustic Analysis of Combustion Instability in a Staged Turbulent Swirled Combustor. *AIAA Journal* , 44(4):741–750, 2006.
- <sup>3</sup>S. R. Stow and A. P. Dowling. Modelling of Circumferential Modal Coupling Due to Helmholtz Resonators. In *ASME Paper 2003-GT-38168*, Atlanta, Georgia, USA, 2003.
- <sup>4</sup>S.R. Stow and A.P. Dowling. A time-domain network model for nonlinear thermoacoustic oscillations. *Journal of Engineering for Gas Turbines and Power*, 131:031502:1–10, 2009.
- <sup>5</sup>F. Nicoud, L. Benoit, C. Sensiau, and T. Poinsot. Acoustic modes in combustors with complex impedances and multidimensional active flames. *AIAA Journal* , 45:426–441, 2007.
- <sup>6</sup>J. Pieringer, T. Sattelmayer, and F. Fassl. Simulation of Combustion Instabilities in Liquid Rocket Engines with Acoustic Perturbation Equations. *Journal of propulsion and power*, 25(5):1020–1031, 2009.
- <sup>7</sup>M. Caraeni, RK Devaki, M. Aroni, M. Oswald, and D. Caraeni. Efficient Acoustic Modal Analysis for Industrial CFD. In *47th AIAA Aerospace Sciences Meeting Including the New Horizons Forum and Aerospace Exposition*. AIAA, 2009.
- <sup>8</sup>C. Pankiewicz and T. Sattelmayer. Time Domain Simulation of Combustion Instabilities in Annular Combustors. *ASME Journal of Engineering for Gas Turbines and Power*, 125(3):677–685, 2003.
- <sup>9</sup>F. Nicoud and K. Wieczorek. About the zero mach number assumption in the calculation of thermoacoustic instability. *International Journal of Spray and Combustion Dynamic*, 1:67–112, 2009.
- <sup>10</sup>K. Wieczorek and F. Nicoud. Thermoacoustic instabilities in non zero Mach number mean flow configurations. In *European Combustion Meeting, Vienna, April 14th-17th*, 2009.
- <sup>11</sup>L. Crocco. Aspects of combustion instability in liquid propellant rocket motors. part i. *J. American Rocket Society* , 21:163–178, 1951.
- <sup>12</sup>L. Crocco. Aspects of combustion instability in liquid propellant rocket motors. part ii. *J. American Rocket Society* , 22:7–16, 1952.
- <sup>13</sup>R. H. Cantrell and R. W. Hart. Interaction between Sound and Flow in Acoustic Cavities: Mass, Momentum, and Energy Considerations. *J. Acous. Soc. Am.* , 36(4):697 – 706, April 1964.
- <sup>14</sup>A. P. Dowling. The Calculation of Thermoacoustic Oscillations. *J. Sound Vib.* , 180(4):557–581, 1995.
- <sup>15</sup>CERFACS. *The AVBP Handbook* - [http://cerfacs.fr/~avbp/AVBP\\_V6.X/HANDBOOK](http://cerfacs.fr/~avbp/AVBP_V6.X/HANDBOOK).
- <sup>16</sup>T. Poinsot and S. Lele. Boundary conditions for direct simulations of compressible viscous flows. *J. Comput. Phys.*, 101(1):104–129, 1992.